Tetrahedron xxx (2014) 1–7

Contents lists available at ScienceDirect

Tetrahedron

journal homepage: www.elsevier.com/locate/tet

A new route towards fluorescent organic nanoparticles with red-shifted emission and increased colloidal stability

Kassem Amro [†], Jonathan Daniel [†], Guillaume Clermont, Talia Bsaibess,
Mathieu Pucheault, Emilie Genin, Michel Vaultier [*], Mireille Blanchard-Desce [*]

Univ. Bordeaux, Institut des Sciences Moléculaires, CNRS-UMR5255, 351 cours de la libération, 33405 Talence, France

ARTICLE INFO

Article history:
Received 31 October 2013
Received in revised form 13 January 2014
Accepted 15 January 2014
Available online xxx

Keywords:
Suzuki coupling
Chromophore
Fluorescence
Nanoparticle

ABSTRACT

Suzuki–Miyaura cross-coupling reaction with a new boron reagent has been used to conveniently and efficiently synthetize a dipolar chromophore having an elongated π-conjugated system (i.e., bithiophene based), which displays a red-shifted emission while maintaining fluorescence. Bright orange emitting FONs made from this 'naked' dipole have been easily prepared and studied. Very interestingly, these FONs with red-shifted emission combine markedly enhanced colloidal and structural stability in water with giant one- and two-photon brightness. As such, they hold promises as fluorescent probes for bioimaging.

© 2014 Published by Elsevier Ltd.

1. Introduction

In last decades, luminescent inorganic nanoparticles based on metals, oxides or semiconductors have attracted a lot of attention for various applications including bioimaging.[1] For such aim, luminescent nanoparticles have to satisfy several criteria. These include high brightness (for enhanced sensitivity with single molecular imaging as an ultimate goal), photostability, colloidal stability as well as biocompatibility. In that respect, luminescent inorganic particles based on semiconductors (i.e., quantum dots) have motivated many studies due to their unique electronic and optical properties. In particular their luminescence properties can be tuned in the visible region by playing on their size.[2,3] They however raises concerns about their environmental toxicity (as the most popular contain heavy metals) and (bio)degradability.

In that context *molecular-based* fluorescent organic nanoparticles (FONs) may provide interesting alternatives as their building blocks can be varied and made to be non-toxic due to their intrinsically versatile structure and formulation. Recently, FONs have attracted increasing interest as they offer promises for a wide range of applications[4,5] including in vivo bioimaging where their specific nanoscale size has been shown for instance to allow sensitive angiography, not accessible to small molecular chromophores.[6]

Because FONs are intrinsically different in nature from quantum dots and polymer nanoparticles, a critical issue is the control of their luminescence properties. In some cases, the fluorescence of chromophoric subunits is quenched in nano-aggregates due to interchromophoric interactions (π-stacking, dimerization) or the onset of non-radiative decay channels competing with fluorescence. In some other cases the switching of the emission properties in FONs is size-dependent and related to the effects from both intermolecular planarization and a specific intermolecular aggregation conformation.[7–10] Hence, the control of FONs luminescence properties requires subtle molecular engineering, taking into account both the electronic properties of the chromophoric subunits and the effect of interchromophoric interactions on their luminescence properties. FONs use in bioimaging also requires high chemical and colloidal stability as their agglomeration in microparticles can be lethal in vivo.[6] Biodegradability and absence of toxicity are additional desired features for FONs to widen their biomedical applicability. In addition, shifting FONs luminescence to the visible red (and further NIR) region is beneficial for bioimaging purposes, as it provides better detection conditions due to reduced scattering in tissues.

Among various dyes, organic π-conjugated dipolar chromophores have been reported as an interesting class of organic dyes liable to form spherical-shaped nanoparticles by spontaneous aggregation in water.[6,11,12] In addition we reported that this strategy was indeed promising as FONs made from such a chromophore (dye **1** in Fig. 1) allowed the preparation of green-emitting FONs,

---

[*] Corresponding authors. Tel.: +33 540006732 (M.B.); tel.: +33 540006731 (M.V.); e-mail addresses: m.vaultier@ism.u-bordeaux1.fr (M. Vaultier), m.blanchard-desce@ism.u-bordeaux1.fr (M. Blanchard-Desce).

[†] K. Amro and J. Daniel contributed equally to the work.

0040-4020/$ – see front matter © 2014 Published by Elsevier Ltd.
http://dx.doi.org/10.1016/j.tet.2014.01.032

Please cite this article in press as: Amro, K.; et al., Tetrahedron (2014), http://dx.doi.org/10.1016/j.tet.2014.01.032

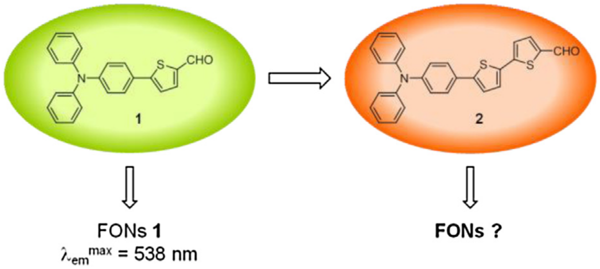

Fig. 1. Structures of dipolar dyes **1** and **2** for elaboration of fluorescent organic nanoparticles (FONs).

which were shown to be non-toxic and allowed acute non-invasive in vivo vascular imaging in small animals (two-photon angiography).[6] These earlier results are clear demonstration of the potential of this type of FONs for biomedical applications. Following this route, we are now aiming at extending their application range by *both* increasing their colloidal stability to a significant extent (FONs made from dye **1** tend to agglomerate over days after their preparation) and shifting their emission to the red region for improved detection in thick samples.

An interesting way of stabilizing organic nanoparticles by using surfactants was demonstrated earlier in the case of polymeric organic nanoparticles.[13] This useful method is yet not always fully desirable for biologic applications due to the potential toxicity or problems with environmental degradability of several synthetic surfactants (such as for instance CTAB or SDS). Earlier attempts to increase colloidal stability of organic nanoparticles made from dipolar (push–pull type) dyes showed that this can possibly be achieved by adding bulky substituents/groups on the molecular units.[11,14] In this paper, we report an alternative and effective, yet synthetically simple way to increase to a dramatic extent the colloidal stability of FONs made from 'naked' dipolar chromophores based on the modification of the electronic structure of the dipolar chromophoric subunits, by extending their π-conjugated system, using oligothiophene conjugated system (Fig. 1). This π-conjugated system allows efficient electronic communication between electroactive end-groups[15] as well as to maintain good photoluminescence properties in extended chromophores built from oligothiophenes.[16] The choice of this π-conjugated system was also meant for red-shifting the luminescence properties towards the visible red with reduced loss of fluorescence intensity.

2. Results and discussion

2.1. Synthesis of the chromophore

The synthesis of compound (**2**) has been realized by Suzuki–Miyaura cross-coupling by following the synthetic route displayed in Scheme 1. Two synthesis of compound (**2**) have been reported earlier: one involves a Stille cross-coupling[17,18] and therefore the use of tin derivatives whereas the second one is based on a Suzuki–Miyaura cross-coupling of 4-(diphenylamino)phenylboronic acid and 5′-iodo-[2,2′]-bithiophenyl-5-carboxaldehyde.[19] Here, we implemented an alternative strategy using a Suzuki–Miyaura cross-coupling between 4-iodophenyldiphenylamine (**c**) and 5′-(4,4,5,5-tetramethyl-[1,3,2]dioxaborolan-2-yl)-[2,2′]bithiophenyl-5 carboxaldehyde (**b**). The Suzuki coupling protocol that we have implemented prevents the short comings (toxicity) associated with the Stille coupling, and differs from the earlier reported Suzuki coupling by the use of reagent (**b**). The advantage of this method lies in the versatility of (**b**). Furthermore, the Suzuki cross-coupling between (**c**) and 5′-formyl-2,2′-bithiophene-5-boronic acid was attempted for comparison purpose: desired product was formed in lower yield and required more tedious purification. 4-Iodophenyldiphenylamine compound (**c**) was easily obtained by a Ullmann coupling reaction involving copper catalyzed iodoarylation of diphenylamine with the 1,4-diiodobenzene.[20] Reagent (**b**) was synthesized by bromination of commercially available [2,2′]bithiophenyl-5-carboxaldehyde with *N*-bromosuccinimide (NBS)[21] leading to brominated derivative (**a**). A subsequent Miyaura borylation reaction of (**a**) with bis(pinacolato)diboron led to pure reagent (**b**) in 40% yield after purification by sublimation and recrystallization from diethyl ether. A further Suzuki–Miyaura cross-coupling between (**b**) and (**c**) in the presence of Pd(OAc)$_2$(5%) and PPh$_3$(15%.) led to the desired aldehyde (**2**) as pure compound in 58% yield, indicating that this route allows efficient synthesis of aldehyde **2**.

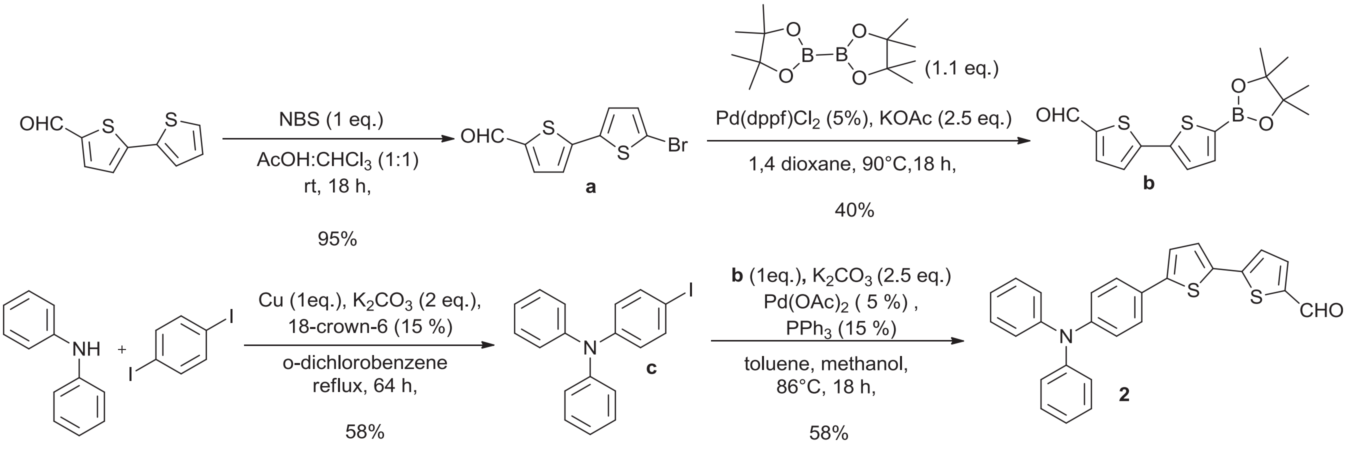

Scheme 1. Alternative multistep synthesis of chromophoric subunit (**2**) using new boronate reagent (**b**).

2.2. Photophysical properties in organic solutions

Photophysical properties of chromophore **2** were first investigated in solution in organic solvents. The photophysical data are collected in Table 1. As chromophore **1**,[6] chromophore **2** displays an intense and broad absorption band in the near UV–blue visible region with a slight bathochromic shift and marked hyperchromic effect compared to compound **1** (Fig. 2). This is consistent with extended electronic conjugation promoted by the bithiophene π-conjugated linker. Interestingly, chromophore **2** also shows

Please cite this article in press as: Amro, K.; et al., Tetrahedron (2014), http://dx.doi.org/10.1016/j.tet.2014.01.032

Table 1
Photophysical characteristics of compound **2**

Solvent	λ_{abs}^{max}/nm	Log ε^{max}/M^{-1} cm^{-1}	λ_{em}^{max}/nm	FWHM/10^3 cm^{-1}	Φ_f[a]	τ_f/Ns[b]
Cyclohexane	417	4.66	476, 508$^{(sh)}$	3.3	0.47	1.0
Toluene	424	4.46	533	3.7	0.71	2.1
$CHCl_3$	431	4.84	589	3.5	0.91	3.1
THF	420	4.56	566	3.6	0.85	2.9
DCM	427	4.64	612	3.5	0.75	3.5
acetone	419	4.55	615	3.8	0.60	3.2
acetonitrile	419	4.73	660	3.9	0.32	2.1
DMSO	430	4.63	670	3.8	0.37	2.2
H_2O (FONs)	422	4.35	597	3.1	0.07[c]	1.1 (0.6) 3.5 (0.4)

[a] Fluorescence quantum yield.
[b] Fluorescence lifetime.
[c] Fluorescence quantum yield measured using an integrating sphere in center-mount holder configuration.

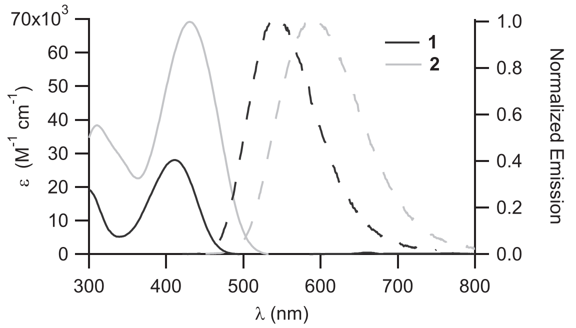

Fig. 2. Absorption and emission spectra of dyes **1** and **2** in chloroform.

significantly red-shifted fluorescence (by about 43 nm in chloroform) compared to that of chromophore **1** while maintaining as high fluorescence quantum yield in low to medium polarity environment (Table 1). Hence the red-shifted emission is not leading to fluorescence decay due to major increase in radiative decay rate (as expected from the large hyperchromic effect).[22]

The larger bathochromic shift of the emission band compared to the red-shift of the absorption band, resulting in larger Stokes shift values, reveals a larger nuclear reorganization in the emissive excited state of **2** as compared to **1**. This indicates a larger electronic redistribution upon excitation, in relation with photo-induced intramolecular charge transfer over longer distance.

Similarly to chromophore **1**,[6] chromophore **2** shows a typical positive solvatochromic behavior typical of an Intramolecular Charge Transfer (ICT) transition with an increase in dipole moment ($\Delta\mu$) upon excitation: the absorption spectra are slightly red-shifted and broadened with increasing solvent polarity while the fluorescence emission shows remarkable bathochromic shifts. The fluorescence emission of compound **2** is tuned from blue-green in low polarity solvents to orange-red in polar solvents (Fig. 3). Hence dye **2** behaves as a microenvironment fluorescent polarity probe. As a result of the solvent-induced spectral shifts, the Stokes shift values are found to increase with solvent polarity (Table 1) following a linear dependency (Fig. 4) on the solvent orientational polarizability function (Δf) as predicted by the Lippert–Mataga relationship (Eq. 1):[23,24]

$$\nu_{abs} - \nu_{em} = 2\left(\Delta\mu^2/hca^3\right)\Delta f + \text{const} \qquad (1)$$

where ν_{abs} (ν_{em}) is the wavenumber of the absorption (fluorescence) maximum, h the Planck constant, c the light velocity, a the radius of the Onsager cavity, and $\Delta f=(\varepsilon-1)/(2\varepsilon+1)-(n^2-1)/(2n^2+1)$, where ε is the dielectric constant and n the refractive

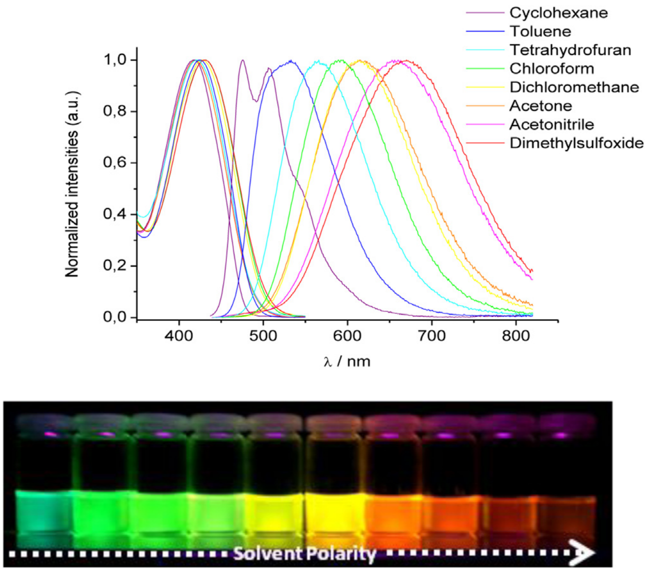

Fig. 3. Top: Normalized absorption and photoluminescence spectra of **2**. Bottom: Illustration of fluorescent polarity probe behavior of compound **2** (λ_{exc}=365 nm).

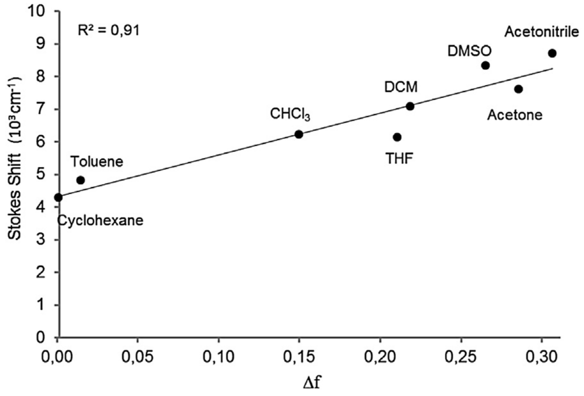

Fig. 4. Lippert–Mataga correlation for compound **2**.

index of the solvent while $\Delta\mu$ is the change of dipole moment of the solute between ground and excited states.

The Onsager cavity radius can be derived from anisotropy and fluorescence lifetime measurements (see Supplementary data)[25] thus allowing the calculation of the photo-induced change of dipole ($\Delta\mu$) of chromophore **2**. Using this protocol, a $\Delta\mu$ value of 15 D is derived for chromophore **2** from the slope values obtained from the Lippert–Mataga linear correlation (i.e., specific shifts $2\Delta\mu^2/hca^3$). A larger $\Delta\mu$ value is derived for chromophore **2** compared to model chromophore **1** (12.5 D see Supplementary data), which further confirms that the bithiophene linker is indeed operative in allowing efficient electronic communication between the electron-donating (NPh_2) and electron-withdrawing (CHO) end-groups.

2.3. Two-photon absorption

Thanks to the fluorescence properties of chromophore **2**, its two-photon absorption (TPA) cross sections in the 700–1000 nm range (i.e., biological spectral window) could be determined in solution by using the two-photon induced fluorescence (TPEF) methodology (Fig. 5).[26] We observe an intense two-photon absorption band located at about half the energy of the lowest one-photon allowed excited state involved in the ICT transition. The TPA band peaks at 910 nm with corresponding maximum TPA cross section of 590 GM, which is more than three times larger than that

Please cite this article in press as: Amro, K.; et al., Tetrahedron (2014), http://dx.doi.org/10.1016/j.tet.2014.01.032

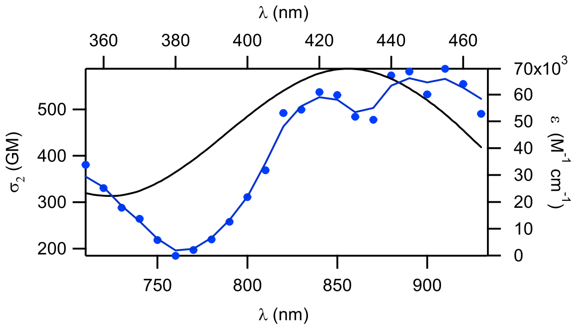

Fig. 5. Two-photon absorption spectrum of chromophore **2** in chloroform (close circles) compared with rescaled one-photon absorption (solid line).

of dye **1**.[6] Hence, the insertion of one extra thiophene ring in the π-conjugated system not only produces red-shifted luminescence but also even stronger hyperchromic effect on 2PA than on one-photon absorption.

2.4. Crystal structure

Single crystals of **2** could be grown by slow evaporation from cyclohexane–dichlomethane mixture and analyzed by X-ray diffraction. As shown in Fig. 6, dipole **2** crystallizes in the triclinic system (space group: P-1). The π-conjugated system linking the donating (NPh_2) and attracting (CHO) end-groups adopts a nearly coplanar conformation between phenyl and thienyl groups. The planarity of the π-connector favors the electronic coupling between the electron-donating and electron-withdrawing end-moieties and facilitates intramolecular charge transfer. We also observed that the two thiophene rings adopt an anti-configuration leading to cis–trans–cis double bonds conjugated system, favorable to increased delocalization. At opposite, the triphenylamine unit adopts a (non-planar) propeller-shape conformation, which hinder close π-stacking and generates a distance of 3.89 Å between the planes of two neighboring molecules. These chromophores adopt an almost perfect antiparallel conformation and are almost ‘sandwiched’ between two perpendicular (and antiparallel) chromophores.

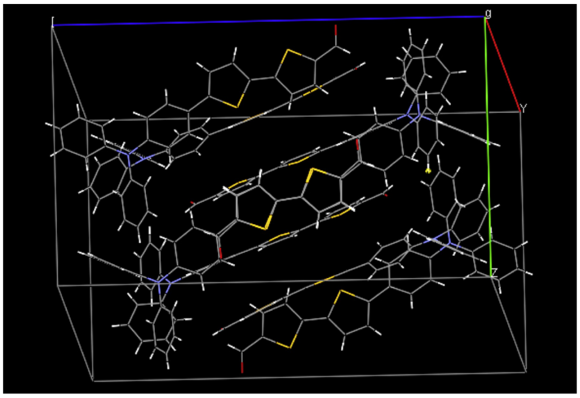

Fig. 6. Molecular structure and crystal packing of dye **2** derived from X-ray diffraction study.

2.5. FONs preparation, stability, and optical properties

FONs made from chromophore **2** were easily prepared using the reprecipitation method. A limpid orange solution was readily obtained after addition of a mM solution of dye **2** dissolved in THF into deionized water. The spontaneous formation of nanoparticles was monitored by absorption spectroscopy. Interestingly, FONs made from dye **2** retain fluorescence and their emission spectrum is similar to that of dye **2** in chloroform solution (Fig. 7). Based on the sensitivity of dye **2** fluorescence on polarity, the luminescence of FONs made from **2** further corroborates the formation of nano-aggregates as the luminescence property indicates that chromophoric subunits experience a medium polarity environment within FONs (intermediary between chloroform and DCM) rather than a polar environment (if they were dissolved as isolated molecules in water).[6] This is further confirmed as the luminescence of crystals (solid state) is observed to be similar to that of FONs in water (see Supplementary data), suggesting the molecules of dye **2** retain, to some extent, the organization of the crystalline state within the nanoparticle. Interestingly, the fluorescence characteristics of FONs made from dyes **2** were found to be independent of their size (see Supplementary data). Both their emission spectra and fluorescence quantum yield remain unaffected, indicating that the emission properties of FONs are essentially originating from the chromophoric subunits.

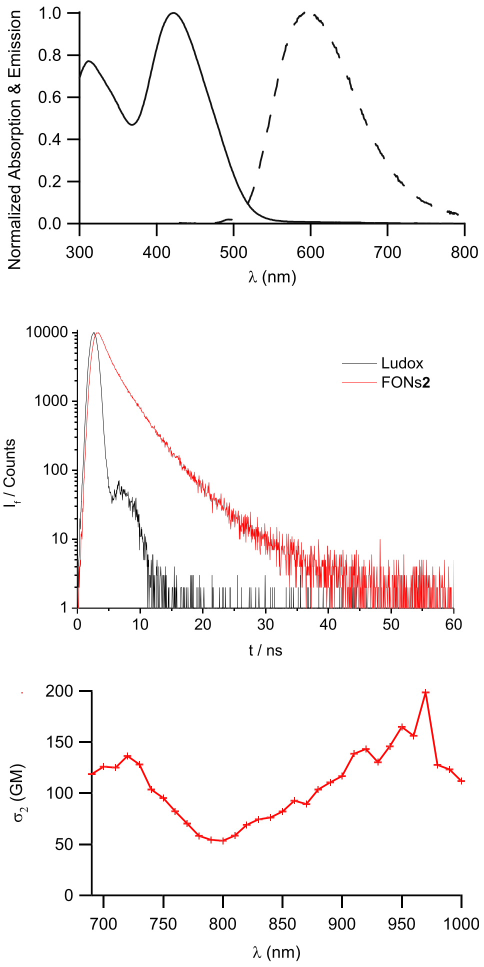

Fig. 7. Top: Normalized absorption and fluorescence spectra of FONs made from dye **2** in water. Middle: Fluorescence decay. Bottom: Two-photon absorption spectrum.

We also observed that FONs made from dye **2** exhibit biexponential fluorescence decay (Fig. 7). The longer lifetime is similar to that of dye **2** dissolved in DCM while the shorter lifetime is indicative of the presence of competitive non-radiative processes. These non-radiative processes, most probably involving dyes lying close to the FONs surface (and thus experiencing the proximity of water molecules favoring vibrational deactivation and/or intermolecular electron transfer), are responsible for the marked

Please cite this article in press as: Amro, K.; et al., Tetrahedron (2014), http://dx.doi.org/10.1016/j.tet.2014.01.032

decrease in fluorescence quantum yield of FONs made from chromophore **2** compared to that of isolated dyes dissolved in chloroform (Table 1).

As dye **2** retains fluorescence as FONs in water, its two-photon absorption spectrum could be determined using the TPEF methodology. As shown in Fig. 7, the TPA band is found to peak at 970 nm and is thus significantly red-shifted compared to that of isolated dye **2** molecule dissolved in chloroform. We also note that the TPA maximum for dye **2** as chromophoric subunits in FONs (200 GM) is reduced by about 65% compared to that determined for dye **2** dissolved in chloroform. These variations are clearly a signature of interchromophoric interactions within the FONs as dipole–dipole interactions have been shown to strongly affect the TPA response of polar and polarizable chromophores (leading to either increase[27–29] or decrease[29,30] of the chromophoric subunits response depending on their relative orientation and positioning) as already reported in model dimeric,[30] multimeric systems,[27–29] and nanoaggregates[6]. This can possibly be attributed to environment and polarization effects (in relation with dipole–dipole interactions, which are stronger in the solid state due to molecular confinement) that affect the TPA response of each chromophoric subunits within FONs.[29,30]

The size and shape of the FONs made from dye **2** was assessed by Transmission Electron Microscopy (TEM) revealing roughly spherical shaped nanoparticles of about 35 nm diameter (Fig. 8). From the size of naked FONs, we could derive the average number of chromophores per FONs and estimate the brightness of the FONs. The data are gathered in Table 2.

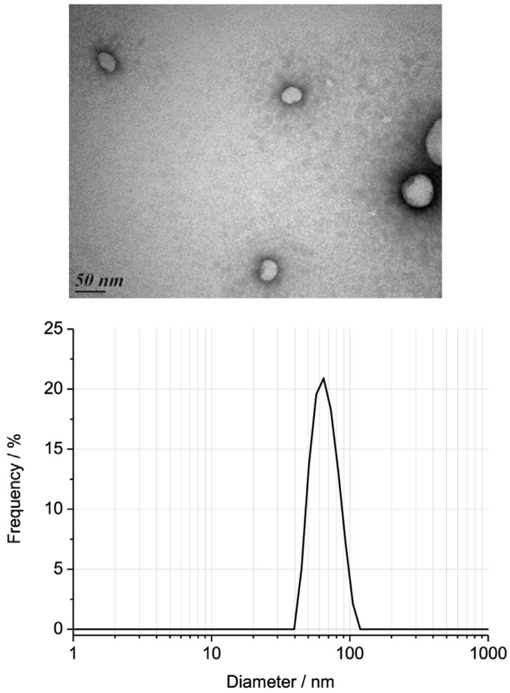

Fig. 8. Top: TEM image of freshly prepared FONs made from dye **2**. Bottom: DLS spectrum of FONs**2** in deionized water.

Table 2
Estimation of the number of chromophores per FON and of the one- and two-photon brightness of FONs made from **2**

R (nm)	N	$\varepsilon^{\max}$ (M^{-1} cm^{-1})	$\sigma_2^{\max}$ (GM)	$\varepsilon^{\max}\,\Phi$ (M^{-1} cm^{-1})	$\sigma_2^{\max}\,\Phi$ (GM)
18	4×10^4	9×10^8	8×10^6	6×10^7	5.5×10^5

Dynamic Light Scattering (DLS) further provided evidence of a unimodal distribution with an average *hydrated* diameter (D_H) of 60 nm with PdI=0.15 (Fig. 8). Interestingly, FONs made from dye **2** were also found to exhibit rather negative zeta potential (−40±5 mV). The larger radius derived from DLS experiments is consistent with FONs having a significant (negative) surface potential, thus generating strong interactions between the FONs surface and dipolar surrounding water molecules.

This negative surface potential is liable to impart good colloidal stability in water. Interestingly, the colloidal stability of FONs made from dye **2** was found to be increased as compared to that of FONs made from dye **1**. This is illustrated in Fig. 9 where the evolution over time of the absorption spectra of FONs**1** and FONs**2** are compared. Whereas FONs made from **1** are found to undergo—after several days—definite size increase as evidenced by increased scattering and decrease of the ICT absorption band at 420 nm (and further attested by DLS study), such phenomenon is found to be significantly reduced in the case of FONs made from dye **2**. Hence lengthening of the conjugated spacer not only leads to significantly red-shifted emission (as required for improved detection in bioimaging) but more surprisingly to increased colloidal stability. This striking effect provides evidence that the colloidal stability can be significantly improved by extending the π-conjugated system in dedicated dipolar chromophores.

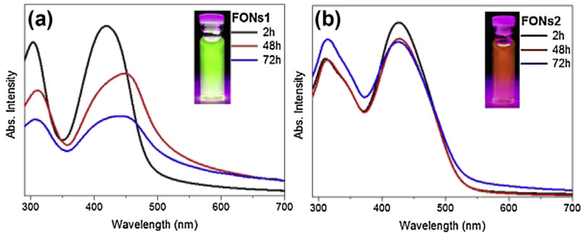

Fig. 9. Evolution of the absorption spectra of FONs made from **1** (a) and **2** (b) in water.

This new finding complements the earlier observation of the markedly different colloidal stabilities of related dipolar and octupolar derivatives[6] and demonstrates that subtle change in electronic distribution in dipolar dyes can also significantly affects the colloidal stability of nanoparticules made from dipolar (and polarizable) organic dyes.

3. Conclusion

An improved and efficient synthesis of dye **2** has been described based on a Suzuki–Miyaura key coupling reaction using a new boron reagent (5′-(4,4,5,5-tetramethyl-[1,3,2]dioxaborolan-2-yl)-[2,2′]bithiophenyl-5 carboxaldehyde). This synthetic strategy avoids the use of toxic reagents required by Stille coupling. Dye **2** was subsequently used to prepare—via a simple and expeditious protocol—novel organic nanoparticles that exhibit bright orange fluorescence emission (λ_{em}~600 nm). These fluorescent nanoparticles of about 35 nm diameter combine giant one- and two-photon brightness ($\varepsilon^{\max}\,\Phi=0.6\cdot10^8$ M^{-1} cm^{-1} and $\sigma_2^{\max}\,\Phi=5.5\cdot10^5$ GM) and good colloidal stability in pure water. As such they hold major promises for bioimaging.

4. Experimental section

4.1. Synthesis

4.1.1. General methods. Commercially available reagents (purchased from Aldrich and Alfa) were used without further purification. Dry solvents were distilled from the appropriate drying

Please cite this article in press as: Amro, K.; et al., Tetrahedron (2014), http://dx.doi.org/10.1016/j.tet.2014.01.032

reagents immediately before use. All air- or water-sensitive reactions were carried out under argon. Reactions were monitored by thin-layer chromatography carried out on silica gel precoated aluminum sheets (60F-254). Column chromatography was performed using Fluka silica gel Si 60 (40–63 μm, 230–400 mesh). Melting points were determined on a STUART SMP 10 digital melting point instrument. Infrared spectra were measured on a Perkin Elmer Spectrum 100 Optica. ^{1}H and ^{13}C NMR spectra were recorded on a Bruker Avance I 300 spectrometer at 300 MHz and 75 MHz, respectively, and on a Bruker Avance III 600 spectrometer at 600 MHz and 150 MHz, respectively. Chemical shifts (δ) are reported in parts per million and residual non-deuterated solvent was used as internal reference. Coupling constants (*J*) are given in Hertz. Mass spectra were performed by the CESAMO (Bordeaux, France). Electrospray (ESI) measurements were carried out on a QStar Elite mass spectrometer (Applied Biosystems). The instrument is equipped with an ESI source and spectra were recorded in the positive mode. The electrospray needle was maintained at 4500 V and operated at room temperature. Samples were introduced by injection through a 20 μL sample loop into a 400 μL/min flow of methanol from the LC pump. Elemental analyses were performed at I.C.S.N– C.N.R.S. (Gif-sur-Yvette, France). Crystallographic data were acquired at CESAMO (Bordeaux, France) using a Bruker APEX 2 DUO instrument. Crystallographic data (excluding structure factors) for the structure in this paper has been deposited with the Cambridge Crystallographic Data Center as supplementary publication nos. CCDC 969193.

*4.1.2. 5′-Bromo-[2,2′]bithiophenyl-5-carboxaldehyde (**a**).*[21] *N*-Bromosuccinimide (2.74 g, 15.4 mmol) was added dropwise under argon to a stirred solution of [2,2′]bithiophenyl-5-carboxaldehyde (3.00 g, 154 mmol) in a 1/1 mixture of $CHCl_3$ (15 mL) and acetic acid (15 mL) kept in the dark at 0 °C. The solution was left to warm to room temperature and stirred overnight. The reaction mixture was then extracted with ethyl acetate (500 mL) and the organic phase was washed with a saturated $NaHCO_3$ solution in water followed by water, then dried over anhydrous Na_2SO_4, and concentrated under vacuum to give (**a**) (4.00 g, 95%) as a yellow solid. ^{1}H NMR ($CDCl_3$, 300 MHz): δ 9.86 (1H, s, C*H*O), 7.65 (1H, d, *J*=3.9 Hz, CHOCC*H*), 7.18 (1H d, *J*=3.9 Hz, CHOCCHC*H*), 7.10 (1H, d, *J*=3.9 Hz, C*H*CHCBr), 7.03(1H, d, *J*=3.9 Hz, 1H, CHC*H*CBr).

*4.1.3. 5′-(4,4,5,5-Tetramethyl-[1,3,2]dioxaborolan-2-yl) [2,2′]bithiophenyl-5-carboxaldehyde (**b**).* 5′-Bromo-[2,2′]bithiophenyl-5-carboxaldehyde (1.88 g, 6.9 mmol) and bis(pinacolato)diboron (1.92 g, 7.5 mmol, 1.1 equiv) were dissolved under argon in anhydrous dioxane (40 mL) in a 100 mL round bottom flask, in which KOAc (1.69 g, 17.2 mmol) and Pd(dppf)Cl_2 (252 mg, 0.3 mmol) were added. The reaction mixture was stirred at 90 °C overnight. After cooling, the mixture was filtered through a pad of Celite, then concentrated under pressure. Crude product was precipitated by addition of diethyl ether then collected by filtration yielding a brown solid. Purification was achieved by sublimation (100 °C, 2.5 mbar), affording analytically pure product (**b**) (820 mg, 40%) as a yellow powder. Mp=148–149 °C; Elemental analysis calcd for $C_{15}H_{17}BO_3S_2$: C 56.26, H 5.35, S 20.03, found: C 56.41, H 5.39, S, 20.35; FTIR (KBr): ν(CHO) 1661 cm^{-1}; ^{1}H NMR ($CDCl_3$, 300 MHz): δ 9.87 (1H, s, C*H*O), 7.67 (1H, d, *J*=3.9 Hz, CHOCC*H*), 7.55 (1H, d, *J*=3.6 Hz, C*H*CHCB), 7.41 (1H, d, *J*=3.6 Hz, CHOCCHC*H*), 7.30 (1H, d, *J*=3.9 Hz, CHC*H*CB), 1.35 (s, 12H); ^{11}B NMR ($CDCl_3$, 96 MHz) 28.2; ^{13}C NMR ($CDCl_3$, 75 MHz) δ 182.5, 146.8, 142.2142.0, 138.1, 137.2, 127.1, 124.9, 84.5, 24.8; HRMS (*m*/*z*) [M] calcd for $C_{15}H_{17}BO_3S_2$ 321.0784, found 321.0797.

*4.1.4. 5′-(4-Diphenylamino-phenyl)-[2,2′]bithiophenyl-5-carboxaldehyde (**2**).*[17,18] 4-Iodophenyl-diphenyl-amine (**c**) (120 mg, 0.33 mmol), 5′-(4,4,5,5-tetramethyl-[1,3,2]dioxaborolan-2-yl)-[2,2′]bithiophenyl-5-carboxaldehyde (**b**) (100 mg, 0.33 mmol) and triphenylphosphine (12 mg, 0.049 mmol) were dissolved under argon in a toluene (1 mL)/methanol (40 μL) mixture. Anhydrous K_2CO_3 (110 mg, 0.82 mmol) and Pd$(OAc)_2$ (4 mg, 0.016 mmol) were added and the reaction mixture was stirred at 86 °C overnight. The reaction mixture was then filtered through a pad of Celite. The filtrate was evaporated under reduced pressure and the residue was purified by silica-gel column chromatography using a 1/1 dichloromethane/petroleum ether mixture to yield 84 mg (58%) of the desired compound (**2**) as an orange solid. Mp=152 °C; ^{1}H NMR ($CDCl_3$, 600 MHz) δ 9.85 (1H, s, C*H*O), 7.66 (1H, d, *J*=3.9 Hz, CHOCC*H*), 7.46 (2H, d, *J*=8.7 Hz, NCCHC*H*), 7.31 (1H, d, *J*=3.8 Hz, CHOCCHCHCCC*H*), 7.28 (4H, t, *J*=7.9 Hz, NCCHC*H*CH), 7.23(1H, d, *J*=3.9 Hz, CHOCCHC*H*), 7.17 (1H, d, *J*=3.5 Hz, CHOCCHCHCCCHC*H*), 7.12 (4H, d, *J*=7.7 Hz, NCC*H*CHCH), 7.05–7.07 (4H, m, NCCHCHC*H*; NCC*H*CH).

4.2. Photophysical and two-photon absorption studies

All photophysical studies have been performed with freshly-prepared air-equilibrated solutions at room temperature (298 K). UV/Vis absorption spectra were recorded on a Jasco V-670 spectrophotometer. Steady-state and time-resolved fluorescence measurements were carried out on a Fluorolog spectrofluorometer. Fully corrected emission spectra were obtained under excitation at the wavelength of the absorption maximum. Fluorescence quantum yields of dilute dye solutions were measured according to literature procedures using fluorescein in 0.1 M aqueous NaOH (Φ=0.90 at 474 nm) or Rhodamine-6G in ethanol (Φ=0.94 at 488 nm) depending on the emission range.[31,32] The reported fluorescence quantum yield values obtained via this method are within ±0.02. Absolute fluorescence quantum yield of the FONs suspension in water was determined using a center-mount sample holder and an integrating sphere. Fluorescence decays were measured in a time-correlated single photon counting (TCSPC) configuration, under excitation from selected nanoLED (370 or 455 nm). The instrument response was determined by measuring the light scattered by a Ludox suspension. The lifetime values were obtained from the reconvolution fit analysis of the decay profiles; the quality of the fits was judged by the reduced χ^2 value ($\chi^2<1.1$). The reported lifetimes are within ±0.1 ns.

Two-photon absorption cross sections (σ_2) were determined from the two-photon excited fluorescence (TPEF) cross sections ($\sigma_2\Phi$) and the fluorescence emission quantum yield (Φ). TPEF cross sections were measured relative to fluorescein in 0.01 M aqueous NaOH in the 715–980 nm spectral range,[26,33] using the method described by Xu and Webb[26] and the appropriate solvent-related refractive index corrections.[34] Reference values between 700 and 715 nm for fluorescein were taken from literature.[35] The quadratic dependence of the fluorescence intensity on the excitation power was checked at all wavelengths. Measurements were conducted using an excitation source delivering fs pulses. This allows avoiding excited-state absorption during the pulse duration, a phenomenon, which has been shown to lead to overestimated two-photon absorption cross-section values. To scan the 680–1080 nm range, a Nd:YVO4-pumped Ti:sapphire oscillator was used generating 140 fs pulses at a 80 MHz rate. The excitation was focused into the cuvette through a microscope objective (10X, NA 0.25). The fluorescence was detected in epifluorescence mode via a dichroic mirror (Chroma 675dcxru) and a barrier filter (Chroma e650sp-2p) by a compact CCD spectrometer module BWTek BTC112E. Total fluorescence intensities were obtained by integrating the corrected emission. The experimental uncertainty of the absorption cross-section values determined from this method has been estimated to be ±10%.

Please cite this article in press as: Amro, K.; et al., Tetrahedron (2014), http://dx.doi.org/10.1016/j.tet.2014.01.032

4.3. Preparation of the FONs

Nanoparticles of chromophores **2** were prepared using the reprecipitation method at room temperature.[36] FONs**2** solution was obtained by dropwise addition of 100 μL of a 1 mM THF solution of compound **2** to 9.9 mL of osmosed water under magnetic stirring. A fluorescent transparent solution is readily obtained after the addition is completed.

4.4. Characterization and zeta-potential analysis of the FONs

TEM was carried out using a HITACHI H7650. The copper grid coated with a carbon membrane was pretreated using the Glow discharge technique to yield positively charged hydrophilic carbon surface to allow stronger interaction between the sample and the grid itself and thus easier imaging. One droplet of the dilute aqueous suspension was deposited on the grid and the excess liquid was drown off with a paper. A staining procedure using uranyl acetate was then used to enhance the contrast.

Dynamic Light Scattering (DLS) was performed using Zetasizer Nano S90 Malvern Instruments operating with a HeNe laser at 90°or SZ-100Z Horiba instrument operating at 173°. The hydrodynamic diameters D_h were calculated from diffusion coefficients using the Stokes–Einstein equation. All correlogram analyses were performed using the software supplied by the manufacturer. The polydispersity index (PdI) is given by the cumulant analysis method. Zeta-potential analysis was performed with the SZ-100Z Horiba instrument. Several measurements were realized for each sample according to a predefined operating procedure.

Acknowledgements

We gratefully acknowledge Conseil Régional d'Aquitaine for financial support (Chaire d'Accueil grant to MBD and X-rays diffraction instrumentation). K.A., J.D., and T.B. received fellowships from GISAMA, Conseil Régional d'Aquitaine and Univ. Bordeaux 1. We thank the Bordeaux Imaging Center-Imagerie Electronique where TEM analysis was performed. A. Lacoudre is thanked for the X-ray crystal structures.

Supplementary data

Supplementary data related to this article can be found at http://dx.doi.org/10.1016/j.tet.2014.01.032.

References and notes

1. Sreenivasan, V. K. A.; Zvyagin, A. V.; Goldys, E. M. *J. Phys.: Condens. Matter* **2013**, *25*, 194101.
2. Smith, A.; Ruan, G.; Rhyner, M.; Nie, S. *Ann. Biomed. Eng.* **2006**, *34*, 3.
3. Yu, W. W.; Qu, L.; Guo, W.; Peng, X. *Chem. Mater.* **2003**, *15*, 2854.
4. Fery-Forgues, S. *Nanoscale* **2013**, *5*, 8428.
5. Patra, A.; Chandaluri, C. G.; Radhakrishnan, T. P. *Nanoscale* **2012**, *4*, 343 and references cited therein.
6. Parthasarathy, V.; Fery-Forgues, S.; Campioli, E.; Recher, G.; Terenziani, F.; Blanchard-Desce, M. *Small* **2011**, *7*, 3219.
7. Fu, H.-B.; Yao, J.-N. *J. Am. Chem. Soc.* **2001**, *123*, 1434.
8. An, B.-K.; Kwon, S.-K.; Jung, S.-D.; Park, S. Y. *J. Am. Chem. Soc.* **2002**, *124*, 14410.
9. Noh, S. B.; Kim, R. H.; Kim, W. J.; Kim, S.; Lee, K.-S.; Cho, N. S.; Shim, H.-K.; Pudavar, H. E.; Prasad, P. N. *J. Mater. Chem.* **2010**, *20*, 7422.
10. Jiang, Y.; Wang, Y.; Hua, J.; Tang, J.; Li, B.; Qian, S.; Tian, H. *Chem. Commun.* **2010**, 4689.
11. Ishow, E. n; Brosseau, A.; Clavier, G.; Nakatani, K.; Tauc, P.; Fiorini-Debuisschert, C. l; Neveu, S.; Sandre, O.; Léaustic, A. *Chem. Mater.* **2008**, *20*, 6597.
12. Zhao, Y. S.; Fu, H.; Peng, A.; Ma, Y.; Xiao, D.; Yao, J. *Adv. Mater.* **2008**, *20*, 2859.
13. Chari, K.; Antalek, B.; Kowalczyk, J.; Eachus, R. S.; Chen, T. *J. Phys. Chem. B* **1999**, *103*, 9867.
14. Campioli, E.; Rouxel, C.; Campanini, M.; Nasi, L.; Blanchard-Desce, M.; Terenziani, F. *Small* **2013**, *9*, 1982.
15. Ripaud, E.; Olivier, Y.; Leriche, P.; Cornil, J.; Roncali, J. *J. Phys. Chem. B* **2011**, *115*, 9379.
16. Capobianco, M. L.; Barbarella, G.; Manetto, A. *Molecules* **2012**, *17*, 910.
17. Chang, Y. J.; Chow, T. J. *Tetrahedron* **2009**, *65*, 4726.
18. Justin Thomas, K. R.; Hsu, Y.-C.; Lin, J. T.; Lee, K.-M.; Ho, K.-C.; Lai, C.-H.; Cheng, Y.-M.; Chou, P.-T. *Chem. Mater.* **2008**, *20*, 1830.
19. Gupta, A.; Ali, A.; Bilic, A.; Gao, M.; Hegedus, K.; Singh, B.; Watkins, S. E.; Wilson, G. J.; Bach, U.; Evans, R. A. *Chem. Commun.* **2012**, 1889.
20. Sissa, C.; Parthasarathy, V.; Drouin-Kucma, D.; Werts, M. H. V.; Blanchard-Desce, M.; Terenziani, F. *Phys. Chem. Chem. Phys.* **2010**, *12*, 11715.
21. Costa, S. P. G.; Batista, R. M. F.; Raposo, M. M. M. *Tetrahedron* **2008**, *64*, 9733.
22. Strickler, S. J.; Berg, R. A. *J. Chem. Phys.* **1962**, *37*, 814.
23. Lippert, E. *Z. Naturforsch., A* **1955**, *10*, 541.
24. Mataga, N.; Kaifu, Y.; Koizumi, M. *Bull. Chem. Soc. Jpn.* **1955**, *28*, 690.
25. Drobizhev, M.; Meng, F.; Rebane, A.; Stepanenko, Y.; Nickel, E.; Spangler, C. W. *J. Phys. Chem. B* **2006**, *110*, 9802.
26. Xu, C.; Webb, W. W. *J. Opt. Soc. Am. B* **1996**, *13*, 481.
27. Terenziani, F.; Parthasarathy, V.; Pla-Quintana, A.; Maishal, T.; Caminade, A.-M.; Majoral, J.-P.; Blanchard-Desce, M. *Angew. Chem., Int. Ed.* **2009**, *48*, 8691.
28. Terenziani, F.; Parthasarathy, V.; Ghosh, S.; Pandey, R.; Das, P. K.; Blanchard-Desce, M. *Proc. SPIE* **2009**, *7413*, 74130M/1.
29. Robin, A.-C.; Parthasarathy, V.; Pla-Quintana, A.; Mongin, O.; Terenziani, F.; Caminade, A.-M.; Majoral, J.-P.; Blanchard-Desce, M. *Proc. SPIE* **2010**, *7774*, 77740N/1.
30. Terenziani, F.; Morone, M.; Gmouh, S.; Blanchard-Desce, M. *ChemPhysChem* **2006**, *7*, 685.
31. Demas, J. N.; Crosby, G. A. *J. Phys. Chem.* **1971**, *75*, 991.
32. Eaton, D. F. *Pure Appl. Chem.* **1988**, *60*, 1107.
33. Albota, M. A.; Xu, C.; Webb, W. W. *Appl. Opt.* **1998**, *37*, 7352.
34. Werts, M. H. V.; Nerambourg, N.; Pélégry, D.; Le Grand, Y.; Blanchard-Desce, M. *Photochem. Photobiol. Sci.* **2005**, *4*, 531.
35. Katan, C.; Tretiak, S.; Werts, M. H. V.; Bain, A. J.; Marsh, R. J.; Leonczek, N.; Nicolaou, N.; Badaeva, E.; Mongin, O.; Blanchard-Desce, M. *J. Phys. Chem. B* **2007**, *111*, 9468.
36. Kasai, H.; Nalwa, H. S.; Oikawa, H.; Okada, S.; Matsuda, H.; Minami, N.; Kakuta, A.; Ono, K.; Mukoh, A.; Nakanishi, H. *Jpn. J. Appl. Phys.* **1992**, *31*, L1132.

Please cite this article in press as: Amro, K.; et al., Tetrahedron (2014), http://dx.doi.org/10.1016/j.tet.2014.01.032